UCLA
UCLA Previously Published Works

Title
Genetic drift suppresses bacterial conjugation in spatially structured populations.

Permalink
https://escholarship.org/uc/item/7g8462gz

Journal
Biophysical journal, 106(4)

ISSN
0006-3495

Authors
Freese, Peter D
Korolev, Kirill S
Jiménez, José I
et al.

Publication Date
2014-02-01

DOI
10.1016/j.bpj.2014.01.012

Peer reviewed

Genetic Drift Suppresses Bacterial Conjugation in Spatially Structured Populations

Peter D. Freese,[†] Kirill S. Korolev,[†‡§¶] José I. Jiménez,[†||] and Irene A. Chen[†**]

[†]FAS Center for Systems Biology and [‡]Department of Physics, Harvard University, Cambridge, Massachusetts; [§]Department of Physics, Massachusetts Institute of Technology, Cambridge, Massachusetts; [¶]Department of Physics and Program in Bioinformatics, Boston University, Boston, Massachusetts; [||]Faculty of Health and Medical Sciences, University of Surrey, United Kingdom; and [**]Department of Chemistry and Biochemistry, Program in Biomolecular Sciences and Engineering, University of California at Santa Barbara, Santa Barbara, California

ABSTRACT   Conjugation is the primary mechanism of horizontal gene transfer that spreads antibiotic resistance among bacteria. Although conjugation normally occurs in surface-associated growth (e.g., biofilms), it has been traditionally studied in well-mixed liquid cultures lacking spatial structure, which is known to affect many evolutionary and ecological processes. Here we visualize spatial patterns of gene transfer mediated by F plasmid conjugation in a colony of *Escherichia coli* growing on solid agar, and we develop a quantitative understanding by spatial extension of traditional mass-action models. We found that spatial structure suppresses conjugation in surface-associated growth because strong genetic drift leads to spatial isolation of donor and recipient cells, restricting conjugation to rare boundaries between donor and recipient strains. These results suggest that ecological strategies, such as enforcement of spatial structure and enhancement of genetic drift, could complement molecular strategies in slowing the spread of antibiotic resistance genes.

INTRODUCTION

Antibiotics are one of the most important medical interventions of the last century. Yet the extensive use of antibiotics has the effect of selecting for resistance among pathogenic bacteria, which already limits treatment of some major types of infection (1). The increase in resistance is primarily driven by the spread of resistance genes already present in natural communities. A major mechanism for horizontal gene transfer is bacterial conjugation (2), which has spread resistance to β-lactams and aminoglycosides to clinically significant organisms (3). The important role of conjugation in the spread of antibiotic resistance, and in microbial evolution in general, motivates both fundamental study of conjugation and strategies to inhibit it.

Conjugation requires physical contact between a donor and recipient cell. The donor cell carries a conjugative plasmid, which contains genes necessary for conjugation and possibly other genes (e.g., encoding antibiotic resistance). A competent donor cell expresses a pilus, which binds to the recipient cell and mediates plasmid DNA transfer. For example, in the well-studied F factor system, an F^+ donor cell transfers the plasmid to the recipient, initially an F^- cell, thus creating a new F^+ transconjugant cell. Conjugation and maintenance of the plasmid slightly reduces organismal fitness, and a large fitness cost is paid in the presence of certain phages (e.g., the filamentous phages including M13, fd, and f1), which attach specifically to the conjugative pilus. Indeed, addition of M13 or its attachment protein, g3p, reduces the rate of conjugation from F^+ cells and could be an interesting strategy to suppress undesired horizontal gene transfer (4,5).

Many clinically and environmentally important habitats are spatially structured because bacteria live in surface-associated colonies and biofilms, where motility is limited (6,7). Although spatial structure is known to play an important role in evolutionary dynamics, its effect on conjugation dynamics has been largely unexplored. Indeed, modeling and experimental studies of conjugation have previously focused on simple well-mixed liquid systems like batch cultures and chemostats, which can be described by mass-reaction equations. These traditional approaches neglect important aspects of natural populations that result from spatial structure. More recently, experimental and theoretical efforts have been directed at studying conjugation in spatially structured environments. Some studies show that conjugation can be quite prevalent in a biofilm (8,9), but others suggest that spread of conjugative plasmids in biofilms and on agar surfaces is quite limited (10,11). When plasmid-bearing cells provide a public good (e.g., by detoxifying Hg^{2+} from their surroundings), the relative frequency of plasmid-bearing and plasmid-free cells also influences the fitness advantage of the plasmid (12). Interpretation of results in spatially structured environments has also been hampered by the difficulty of distinguishing among donor, recipient, and transconjugant cells by microscopy. In general, previous methods have not been able to resolve two of the three cell types in situ (13). Thus, these experimental results, which are affected by multiple factors (e.g., cell densities, plasmid characteristics, and the spatial scale of structuring), point toward a need for improved experimental systems as well as a quantitative theoretical framework to advance our fundamental understanding of conjugation.

Models developed to describe homogeneous environments do not properly capture dynamics on heterogeneous

environments (14–16). Early models of conjugation in spatially structured environments included unrealistic assumptions or did not allow measurement of transfer events per donor-recipient encounter, which is necessary for comparison of conjugation rates across different species and situations (13,17,18). A more recent spatial model of conjugation (19) used cellular automata to simulate individual cells in a lattice and captured features of experimental conjugation. Although this analysis considered the possibility of local plasmid extinction, it was unable to completely determine genetic history during colony expansion experiments, because donors and transconjugants could not be discriminated in situ. This history is important because in spatially structured populations, only a small number of nearby cells compete with each other, leading to substantial demographic stochasticity (genetic drift) on short spatial scales (20). As a result, some genotypes become extinct locally, leading to a macroscopic pattern of isogenic domains (sectors) in a growing bacterial colony. The number of sectors tends to decrease over time because sectors irreversibly disappear due to genetic drift when sector boundaries cross. We hypothesized that this spatial demixing of genotypes could profoundly affect bacterial conjugation because plasmid transfer requires spatial proximity of the donor and recipient cells.

In this study, we explored the dynamics of bacterial conjugation in colonies grown on an agar surface by combining spatially resolved measurements and simulations. We visualized the spatial distribution of donor cells (F^+ encoding tetracycline resistance, i.e., Tc^r, with cyan fluorescent protein expressed from a nonconjugative plasmid) and recipient cells (initially F^-, tetracycline-sensitive Tc^s, with yellow fluorescent protein expressed from a nonconjugative plasmid). Because the Tc^r phenotype is carried on the F plasmid, transconjugants are Tc^r yellow fluorescent cells. Populations of transconjugants could be visually distinguished from F^- cells by a decrease in fluorescence intensity caused by partial repression of the fluorescent protein, as well as by tetracycline resistance. Contrary to the general belief that biofilms facilitate conjugation, we found that conjugation is substantially suppressed in surface growth compared to liquid culture, consistent with simulations of conjugation dynamics. Thus, spatial structure itself could be an important factor in slowing down the spread of antibiotic resistance. In addition, previous studies in liquid culture showed that exogenous addition of M13 phage particles or the soluble portion of the M13 minor coat protein g3p (g3p-N) results in nearly complete inhibition of conjugation (4,5). We found a similar inhibitory effect of g3p-N in surface-associated bacterial colonies. The work presented here adds to prior experimental and theoretical studies of conjugation on spatially structured environments by quantifying genetic drift, which accounts for the limited penetration of the F plasmid into the spatially structured environment, and by analyzing conjugation rates in the presence of an inhibitory agent. The results suggest that molecular anticonjugation strategies could generalize to natural spatially structured populations.

MATERIALS AND METHODS

Bacterial strains and culture

E. coli TOP10F′ and TOP10 (*mcrA Δ(mrr-hsdRMS-mcrBC) Φ80lacZΔM15 ΔlacX74 recA1 araD 139 (ara leu) 7697 galU galK rpsL (StrR) endA1 nupG*, obtained from Invitrogen, Carlsbad, CA) were used as donor (F^+_c) or recipient (F^-), respectively, of the F′ plasmid (*lacI^q, Tn10(tet^R)*). Plasmids pTrc99A-eYFP (amp^R) and pTrc99A-eCFP (amp^R) encoding, respectively, eYFP (Q95M, yellow) and eCFP (A206K, cyan) were courtesy of Howard Berg. The fluorescent markers were expressed from amp^R selectable plasmids under an isopropyl-β-D-1-thiogalactopyranoside (IPTG)-inducible promoter.

Standard protocols were used for common bacterial and phage-related procedures (21). All strains were grown in Luria-Bertani (LB) medium on a regular basis. When needed, media were supplemented with ampicillin or carbenicillin (100 μg/mL), tetracycline (12 μg/mL), and IPTG (1 mM). Agar plates were made with 20 mL LB supplemented with carbenicillin and IPTG. Separate 3-mL overnight cultures of TOP10F′ (transformed by pTrc99A-eCFP) and TOP10 (transformed by pTrc99A-eYFP) were inoculated in 3 mL of LB with ampicillin, ITPG, and tetracycline if appropriate. Overnight cultures were inoculated from a colony grown on medium with the appropriate antibiotic(s) to select for the desired plasmids, and grown at 37°C with shaking at 250 rpm overnight to saturation (OD$_{600}$ ~ 3–4 was determined by an Ultrospec cell density meter; GE Healthcare, Pittsburgh, PA). F^+ cells grown in medium supplemented with antibiotics were centrifuged for 5 min at 5000 rpm, the supernatant was discarded, and the pellet was resuspended in fresh LB medium lacking antibiotics. Cultures were diluted for density measurement with appropriate medium to bring the OD$_{600}$ within the linear range of the cell density meter (i.e., <1 OD units). Strains were then mixed to the desired ratio as measured by optical density to create the inoculant. A small volume of inoculant (1–20 μL) was pipetted onto the center of an LB-agar plate containing carbenicillin and IPTG. The plates were then incubated for the desired length of time at 37°C in a bin containing wet paper towels to maintain high humidity.

Detection of transconjugants

After the desired growth period, transconjugants were detected by applying a tetracycline-soaked ring around the bacterial colony. The center of a 2.5-cm-diameter filter paper disk (VWR, Bridgeport, NJ) was removed to create a thin annulus with inner diameter 1.9 cm. Tetracycline stock at 12 mg/mL was diluted to 2 mg/mL with 50% ethanol. A quantity of 30 μL of the tetracycline mixture was applied uniformly onto an autoclaved filter paper annulus, which was then placed around a growing bacterial colony with sterilized forceps. Because the number of sector boundaries is not very large, the number and size of transconjugant sectors is expected to vary from colony to colony even though there are millions of cells growing on a petri dish. We indeed observed much higher variability in spatial compared to liquid assays of conjugation and performed measurements on 10–100 colonies in each experiment to obtain reliable estimates of the averages.

Application of g3p-N

The g3p-N protein was prepared as described in Lin et al. (5). A quantity of 4.9 μL of g3p-N stock solution (41 μM) was mixed with 45 μL of phosphate-buffered saline per plate and a 50-μL aliquot was spread on

each plate with glass beads for 1–2 min until dry. Assuming uniform diffusion throughout the 20-mL agar plate, the expected [g3p-N] is 10 nM, a concentration that gives 80% conjugation inhibition in liquid culture (5).

Microscopy and image processing

Fluorescent images were obtained with a Lumar V.12 fluorescence stereoscope (Zeiss, Oberkochen, Germany) and a Typhoon TRIO variable-mode imager (GE Healthcare). Scanned plates were imaged from the bottom using cyan laser excitation and detection at 488 nm with 50-μm resolution. The initial radii of the colonies were measured within 1 h of inoculation by fitting of a circle using the stereoscope's software; colonies that were not circular were discarded. The numbers of sectors in each colony were counted manually. The software MATLAB R2010 (The MathWorks, Natick, MA) was used to extract the radii and sector boundaries of the colonies using the built-in edge-function.

Modeling and simulations of conjugation in bacterial colonies

We formulated a minimal model of surface-associated populations. Following the stepping-stone model of Kimura and Weiss (22), spatially structured populations are often modeled as an array of well-mixed populations (demes) that exchange migrants. Previous work demonstrated that genetic demixing in growing bacterial colonies can be described by a one-dimensional stepping-stone model because growth occurs only close to the nutrient-rich circumference of the colony (23,24). Here, we formulated a model that, in addition to competition, genetic drift, and migration, incorporates horizontal gene transfer between cells. Because previous work showed that the qualitative behavior of linearly and radially expanding populations is quite similar, and both types of expansions lead to sector formation (23), we, for simplicity, neglected the fact that the circumference of the colony, and therefore the total population size, were changing during the experiment.

In our study, simulated populations were composed of a linear set of L_{sim} demes containing N cells of three possible types: F⁻, F⁺$_c$, and transconjugants with respective proportions f^-, f^+_c, and f^t. Each deme was treated as a well-mixed population. To account for daughter cells being displaced slightly from parent cells during colony growth, cells could migrate to one of their two nearest-neighbor demes with probability m per generation. Reproduction and conjugation were modeled through a series of time steps at which only two cells were updated, always preserving the total population size. In reproduction events, one individual died (or fell behind the expanding front in the context of our experiments), allowing another individual to reproduce and thus keep the population size constant. A series of N time steps corresponded to one generation because every individual was replaced once on average.

Possible composition-changing events are given below with their corresponding probabilities P, which depend on the fitness cost s of the F plasmid, conjugation rate r, and the local proportions of the cell types F⁻ (f^-), original cyan F⁺$_c$ (f^+_c), and transconjugant (f^t). These probabilities (see Eqs. 1–6 below) were formulated assuming that conjugation and competition occur at a fixed probability per cell-cell interaction within each deme. Conjugation events decrease the F⁻ population and increase the transconjugant population, whereas competition decreases the F⁺ populations (donor strain and transconjugants) and increases the F⁻ population because the F plasmid imposes a fitness cost. For example, in Eq. 1 below, the probability that the F⁻ population increases by one cell and the F⁺$_c$ population decreases by one cell is proportional to the probability of F⁻ and F⁺$_c$ interaction given by the product of their proportions ($f^- * f^+_c$) and the sum of three terms describing genetic drift (factor of 1), competition ($s/2$), and conjugation ($-r/2$). As expected, this probability increases as the fitness cost of the F plasmid increases, and decreases as the conjugation rate increases:

$$P\left(f^- + \frac{1}{N}, f^+_c - \frac{1}{N}, f^t\right) = f^- f^+_c \left(1 + \frac{s}{2} - \frac{r}{2}\right), \quad (1)$$

$$P\left(f^- - \frac{1}{N}, f^+_c + \frac{1}{N}, f^t\right) = f^- f^+_c \left(1 - \frac{s}{2} - \frac{r}{2}\right), \quad (2)$$

$$P\left(f^- + \frac{1}{N}, f^+_c, f^t - \frac{1}{N}\right) = f^- f^t \left(1 + \frac{s}{2} - \frac{r}{2}\right), \quad (3)$$

$$P\left(f^- - \frac{1}{N}, f^+_c, f^t + \frac{1}{N}\right) = f^- f^+_c r + f^- f^t \left(1 - \frac{s}{2} + \frac{r}{2}\right), \quad (4)$$

$$P\left(f^-, f^+_c + \frac{1}{N}, f^t - \frac{1}{N}\right) = f^t f^+_c, \quad (5)$$

$$P\left(f^-, f^+_c - \frac{1}{N}, f^t + \frac{1}{N}\right) = f^t f^+_c. \quad (6)$$

In the limit of infinite population size, when fluctuations can be neglected, one can obtain a simple description of the dynamics in terms of ordinary differential equations. The key idea is to compute the average change in the relative proportions of the different cell types using Eqs. 1–6 and then treat f^-, f^+_c, and f^t as deterministic variables. For example, the change of f^- per one time step ($1/N$ of generation time) is given by

$$E\left[\frac{1}{N}\left(\begin{array}{c} \left(P\left(f^- + \frac{1}{N}, f^+_c - \frac{1}{N}, f^t\right) - P\left(f^- - \frac{1}{N}, f^+_c + \frac{1}{N}, f^t\right)\right) \\ + P\left(f^- + \frac{1}{N}, f^+_c, f^t - \frac{1}{N}\right) - P\left(f^- - \frac{1}{N}, f^+_c, f^t + \frac{1}{N}\right) \end{array}\right)\right]$$

$$= \frac{1}{N}\left(f^- f^+_c \left(1 + \frac{s}{2} - \frac{r}{2}\right) - f^- f^+_c \left(1 - \frac{s}{2} - \frac{r}{2}\right)\right.$$

$$\left. + f^- f^t \left(1 + \frac{s}{2} - \frac{r}{2}\right) - \left(f^- f^+_c r + f^- f^t \left(1 - \frac{s}{2} + \frac{r}{2}\right)\right)\right)$$

$$= \frac{1}{N}(s - r)f^-(t)\left[f^+_c(t) + f^t(t)\right],$$

which is the combined effect of the four possible transitions that change the number of F⁻ cells. After dividing by the time interval $1/N$, and repeating the same calculation for f^+_c and f^t, we obtain the following set of differential equations:

$$\frac{d}{dt}f^-(t) = (s - r)f^-(t)\left[f^+_c(t) + f^t(t)\right], \quad (7)$$

$$\frac{d}{dt}f^+_c(t) = -sf^-(t)f^+_c(t), \quad (8)$$

$$\frac{d}{dt}f^t(t) = (r - s)f^-(t)f^t(t) + rf^-(t)f^+_c(t). \quad (9)$$

The terms in Eq. 7 allow straightforward interpretation: F^- cells increase due to selection at rate s and decrease due to conjugation at rate r, both of which occur proportional to the frequency at which F^- and F^+ cells come together. Equations 8 and 9 allow analogous interpretation in terms of appropriate events that change the number of F^+_c and transconjugant cells.

Multiple choices of transition probabilities lead to the same behavior in the limit of infinite population size. However, the choice does not affect the dynamics provided that $s \ll 1$ and $r \ll 1$, as is reasonable here, and that the dynamics are equivalent to the Moran model (25) of three neutral species for $s = r = 0$. The reason is that the full dynamics of the cells can be described by stochastic differential equations with the deterministic terms given by Eqs. 7–9 while dependence of the stochastic terms on s and r can be neglected.

After the N time steps of reproduction and conjugation events, migration was implemented such that demes were chosen for migration in random order. When a deme was chosen, each of the N individuals was sequentially selected and migrated to the right deme with probability $m/2$ and to the left deme with probability $m/2$. If the individual was chosen to migrate, a random individual from the destination migrated back to the origin so that the population size in each deme was always conserved. To avoid edge artifacts and to mimic the actual experiments, we imposed periodic boundary conditions so that a cell could migrate from the last deme to the first deme and vice versa. Further details of the model are provided in Methods: Modeling Details in the Supporting Material.

Parameterizing the model

To use the model for quantitative predictions, we parameterized the model using experimental data. We employed the model to estimate the effective conjugation rate in our experimental populations by finding the model parameters that lead to the same spatial distribution of F^-, F^+_c, and transconjugant cells as observed in the experiments. The process of parameterizing the model is quite straightforward, provided the following three issues are taken into account:

1. Spatial patterns are stochastic in both simulations and experiments, so the model should fit average properties of these patterns rather than patterns themselves.
2. Not all parameters in the simulation can be determined uniquely, because the choice of spatial and temporal scales in the simulations depends on the level of desired precision or coarse-graining that can be freely adjusted.
3. Our simulations have a constant length, whereas the circumference of the colonies increases with time, so the process of comparing the patterns has to take these differences in the geometry into account.

We now briefly outline the parameter fitting procedure (also see Table 1); for the complete description, see Methods: Modeling Details in the Supporting Material.

The spatial patterns that result from genetic drift and competition have been previously investigated in Korolev et al. (23,24,26), where the authors showed the population dynamics without conjugation that we study here can be described in terms of the following three quantities:

1. Effective diffusion constant,

$$D_s \sim m * (\text{deme size}) / (\text{generation time}).$$

2. Effective strength of genetic drift,

$$D_g \sim (\text{deme size}) / (N * \text{generation time}).$$

3. Outward bending of more fit sectors,

$$v_\perp \sim s * (\text{deme size}) / (\text{generation time}).$$

Korolev et al. (23,24,26) have computed various statistics based on the spatial patterns of genetic demixing and competition that can be used to estimate these three parameters. Here we omit the derivations of their published results and only provide the mathematical expressions used in the analysis.

Quantifying migration, genetic drift, and the fitness cost of the F plasmid

Procedures for quantifying migration, genetic drift, and the fitness cost of the F plasmid are given in Methods: Modeling Details in the Supporting Material.

Connecting experiments with simulations

The experiments have definite physical measures of time and space, but these are arbitrarily scaled in simulations. For computational efficiency, we used this freedom in choosing spatial and temporal scales to select certain values of m and N ($N = 100$, $mN = 5$) and then determined the corresponding spatial and temporal scales by matching experimental and simulation data. As we show in Data: Simulation Details in the Supporting Material, this choice does not affect our estimate of the conjugation rate, which we further verified by repeating model parameterization for different values of m and N ($N = 30$, $mN = 1$ and $N = 30$, $mN = 10$). To match experimental and simulation data, we defined four dimensionless quantities (invariants, Inv) derived from the six experimental parameters D_g, D_s, $v_\perp$, $\langle f^t \rangle$ (average fraction of transconjugants), T_{exp} (total time), and L_{exp} (population front length):

$$Inv_1 = \frac{D_s}{D_g^2 T_{\text{exp}}}, \tag{10}$$

$$Inv_2 = \frac{D_s}{D_g L_{\text{exp}}}, \tag{11}$$

$$Inv_3 = \frac{v_\perp T_{\text{exp}}}{L_{\text{exp}}}, \tag{12}$$

TABLE 1 Parameterization sources

Parameter	Experimental data	Simulation data
Migration (D_s)	Wandering of sector boundaries	Global heterozygosity (probability that two cells from the colony are the same type)
Genetic drift (D_g)	Number of surviving sectors	Local heterozygosity (probability that two cells from a deme are the same type)
Cost of the conjugative plasmid (s)	Bending of sector boundaries	Bending of sector boundaries
Spatial and temporal scales	Measured distance and time	Deme number and size

Description of model parameters and their analogs in experimental and simulation data. Parameters were combined to calculate dimensionless invariants, as described in the Materials and Methods, to match experimental and simulation data.

$$Inv_4 = \langle f^t \rangle. \tag{13}$$

To establish a match, the values of these experimental invariants and their simulation counterparts must be equal. In particular, the first two invariants were used to find the number of simulation generations and demes (T_{sim} and L_{sim}, respectively). The third invariant was used to estimate the fitness cost of the plasmid, and the fourth invariant to estimate the conjugation rate.

RESULTS

Visualizing conjugation during colony expansion

To visualize conjugation, we began experiments with F^+ donor cells expressing eCFP (enhanced cyan fluorescent protein) and F^- recipient cells expressing eYFP (enhanced yellow fluorescent protein). The two strains were grown to saturation overnight, mixed to the desired proportion (generally 1:1 F^+: F^-) by optical density, inoculated onto agar plates in drops of 1–20 μL, and incubated at 37°C. The schematic of the experiment is shown in Fig. 1 A and expansion
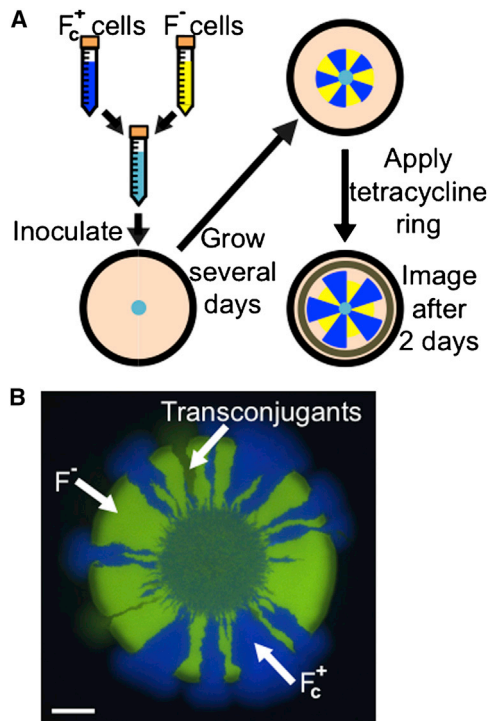

FIGURE 1 Experimental setup. (A) F^- and F^+_c liquid cultures were grown to saturation overnight, mixed to the desired ratio (most often 1:1) as measured by optical density, and 1–20 μL was pipetted onto an agar plate. After 4–7 days of growth, a ring of tetracycline was applied around the colony, which diffused through the agar and allowed only F^+ and transconjugants to grow for two more days. Fluorescence microscopy revealed transconjugants as yellow sectors that continued to grow after tetracycline application. (B) A mixed colony was grown for four days before tetracycline application, followed by two days of additional growth. The inner circle is the drop of the initial inoculant (1 μL). Once tetracycline is applied, only the F^+_c cells and dark-yellow transconjugants continue to grow. The tetracycline ring is outside the field of view. Scale bar is 1 mm. To see this figure in color, go online.

rates in Fig. S1 in the Supporting Material. The spatial distribution of F^+ donor cells and initially F^- cells was visualized by fluorescence microscopy. However, both transconjugant cells and F^- cells express eYFP, so we applied a ring of filter paper soaked in tetracycline to identify the Tc^r transconjugants. Because only F^+ cells are able to grow in the presence of tetracycline (tet^R being carried on the F plasmid), transconjugant sectors appeared as yellow fluorescent sectors that continued to grow after the application of tetracycline (Fig. 1 B). In the following, we refer to cyan fluorescent F^+ cells as "F^+_c", yellow fluorescent F^- cells as "F^-", and yellow fluorescent F^+ cells as "transconjugants".

We observed that the application of tetracycline caused a decrease in the fluorescence intensity of transconjugant cells, as illustrated by the difference between transconjugant and F^- cells (Fig. 1 B). This decrease is attributed to the laI^q being carried on the F plasmid that partially represses expression of the fluorescent protein, which is under an IPTG-inducible promoter. This intensity effect enables visualization of the boundaries of the transconjugant sector so the transconjugant can be traced back to its origin, presumably close to the conjugation event.

A key feature of the spatial dynamics is the formation of monochromatic sectors composed of cells descending from either cyan or yellow fluorescent ancestors (Fig. 1 B). Although a large number of individuals comprise the population, only a small number of individuals reproduce locally (i.e., at the nutrient-rich colony edge), leading to strong genetic drift. These demographic fluctuations reduce genetic diversity at the growing front and result in a single genotype reaching fixation locally and forming a small monochromatic domain. Over time, some of these domains grow whereas others disappear due to the random walk-like motion of the sector boundaries. Transconjugant sectors originate exclusively between a sector of F^+ and F^- cells because conjugation can only occur when F^+ and F^- cells are in physical contact.

Limited spread of F plasmid in spatially structured populations

The fate of the F plasmid depends on whether it can spread in a population. The rate of spread is determined by the fitness advantage or disadvantage conferred by the F plasmid and by the rate of plasmid transfer from F^+ to F^- cells during conjugation. In the presence of tetracycline, the F plasmid confers a strong growth advantage and spreads in the population due to the increase in the number of F^+ cells, including transconjugants, relative to F^- cells. In the absence of tetracycline, the F plasmid imposes a metabolic cost on its host (27); therefore, to survive it must spread through conjugation faster than F^- cells outcompete F^+ cells. Previous experiments in the same system showed that the F plasmid spreads rapidly in

exponentially growing, well-mixed liquid cultures without tetracycline (5), in which the transconjugant fraction approaches 1 at a rate of 0.42 h^{-1}. In striking contrast, we saw that the fraction of cells with the plasmid stayed approximately constant or even slightly declined over time in a spatially structured population (Fig. 2; compare with Fig. 1 from Lin et al. (5), reprinted as Fig. S2). This qualitative change in the fate of the F plasmid shows that conjugation studied in well-mixed liquid cultures is a poor analog for conjugation in surface-associated colonies that more closely resemble natural populations.

Accelerated loss of F plasmid in the presence of g3p

To test whether molecular strategies for inhibiting conjugation were effective in the spatially structured population, we experimentally inhibited conjugation with a soluble form of the g3p protein of the M13 bacteriophage (g3p-N). At a protein concentration that decreases conjugation by 80% in liquid medium, the proportion of transconjugant cells at the colony front decreased by ~69% (from 5.2 to 1.6%, measured by circumference; Fig. 3). In addition, the average number of transconjugant sectors decreased by ~53% (from 2.1 to 1.0, see Fig. S3), confirming that g3p-N protein can indeed inhibit conjugation in surface-associated populations as well as in well-mixed populations.

Model of conjugation in spatially structured populations

We extended the one-dimensional stepping-stone model of colony expansion to include conjugation. In the spirit of the Moran model (25) of evolution at constant population

FIGURE 3   Cell types with and without conjugation inhibition by g3p-N. Circumference proportion of each cell type after four days of growth for 1:1 F$^+$F$^-$ colonies (1 μL inoculum). The average proportion of transconjugants decreased threefold from 5.2 $\pm$ 1.0% to 1.6 $\pm$ 0.4% with addition of g3p. Data shown are mean $\pm$ SE of $n = 44$ colonies without g3p-N and $n = 28$ colonies with g3p-N. To see this figure in color, go online.

size, in which one individual reproduces and one individual dies during each time step, each generation consisted of a series of updates at which two cells were considered. As with previous modeling in this framework (23), these cells could exchange positions during a migration event, or one cell could die while the other divides during a reproduction event. In addition, here we introduced the possibility that one cell could transfer a plasmid to another during a conjugation event. The probabilities of these events were parameterized by the migration rate m, fitness cost of the F plasmid s, and conjugation rate r. The strength of genetic drift was controlled by N, the population size of each deme. The simulations were initialized by populating the demes with F$^+$ and F$^-$ cells drawn with equal probability. This procedure was similar to the well-mixed initial conditions in the experiments.

Our simple model (Fig. 4, *A* and *B*) qualitatively captured the experimentally observed formation of sectors and the appearance of transconjugant sectors (Fig. 4 *C*). As in the experiments, we found that transconjugant sectors appeared between sectors of F$^+$ and F$^-$ cells, and that the number of transconjugant cells was smaller in spatial populations compared to well-mixed populations, suggesting that spatial structure could at least partially explain the stark difference in the fate of the F plasmid between liquid cultures and surface-associated colonies.

Quantification of genetic drift and migration

Genetic demixing, the most prominent feature of evolutionary dynamics in bacterial colonies, is controlled by the strength of genetic drift and migration. We quantified migration by D_s, the effective diffusion constant of sector boundaries, and genetic drift by D_g, the inverse of the product of the effective population density and the
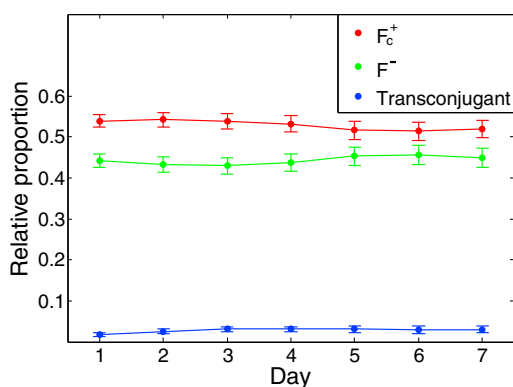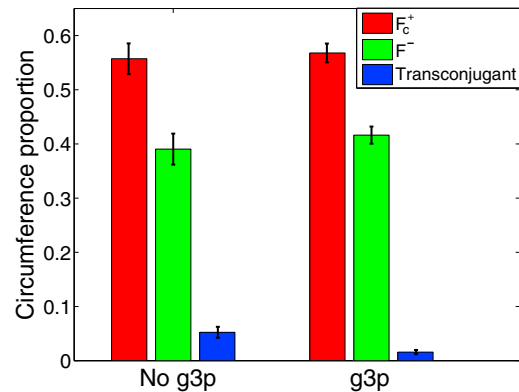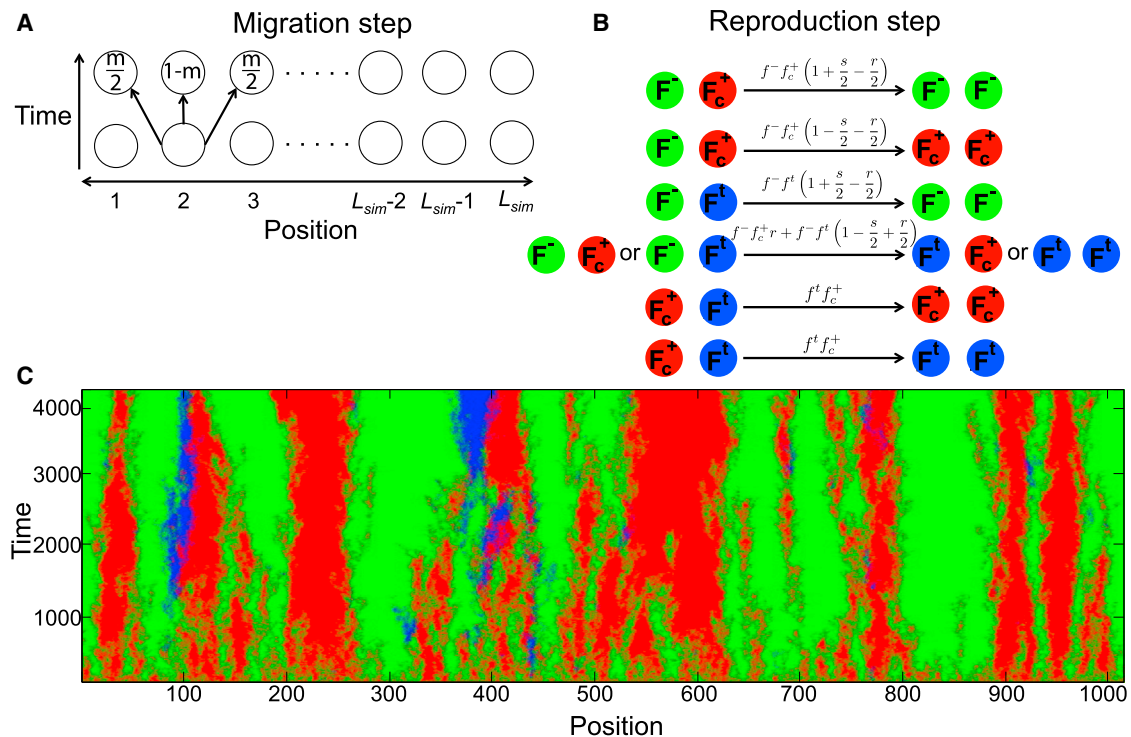

FIGURE 2   Dynamics of cell types in a conjugating spatially structured population. In contrast to the rapid ascension of transconjugants in well-mixed culture, transconjugants in spatial populations remain a small fraction of the population, because conjugation events are limited to the few boundaries between F$^+$ and F$^-$ sectors. The radial position of day x was inferred as $x/7$ of total radial expansion during one-week growth without tetracycline. Data shown are mean $\pm$ standard error (SE) of $n = 35$ colonies (1 μL inoculum). To see this figure in color, go online.

FIGURE 4 Simulation of conjugation during surface-associated growth. (*A*) Overview of the simulation: growth of the colony's population front-outward over time is modeled by L_{sim} demes with N individuals each (indexed linearly with periodic boundary conditions). At the end of a generation, each individual migrates to either adjacent deme with probability $m/2$. (*B*) At each generation, all individuals are sequentially selected and undergo birth and death, which include selection (*s*) and conjugation (*r*) according to the transition probabilities per generation (Eqs. 1–6) and the availability of interacting partners within the same deme. The probabilities in panel *B* do not sum up to one because some events do not change the composition of the population and therefore are not shown. (*C*) Simulated expansion shows good qualitative agreement with the experiments. This visualization with indexed deme position on the *x* axis and generation number on the *y* axis mimics experiments with F^+_c cells (shown as *red* here), F^- (*green*), and transconjugants (*blue*). Parameters correspond to the $N = 100$, $mN = 5$ simulation set in Table S4 in the Supporting Material. To see this figure in color, go online.

generation time. Here we followed the approach that has been previously applied to nonconjugating surface-associated microbial populations (24). For simplicity of the analysis, we performed experiments with two F^- strains with different fluorescent colors because this avoids the complications of both the fitness cost of the F plasmid and conjugation.

We confirmed that experimental data indeed satisfied Eq. S3 in the Supporting Material and found $D_s/v_{||} = 32$ μm (Fig. 5 *A*). Note that the expansion velocity $v_{||} = 0.4$ mm/day, and initial sector boundary position R_i (varying from colony to colony and boundary to boundary), were both measured directly (see Materials and Methods; and see Fig. S1). D_s was also measured from simulations according to Eq. S4 in the Supporting Material (see also Table S1 and Fig. S4, Fig. S5, and Fig. S6 in the Supporting Material).

The strength of genetic drift was measured experimentally according to Eq. S5 in the Supporting Material, which predicts that the number of sectors grows as the square root of the initial colony radius. We varied R_0 by inoculating the colonies with different amounts of well-mixed liquid culture and confirmed the square-root dependence (Fig. 5 *B* and see

Fig. S7). Then, $D_g/v_{||} = 0.785$ was estimated by fitting Eq. S5 in the Supporting Material to the data using our previous estimate of D_s. The fit to the simulation data also yields an estimate of D_g, as described in the Materials and Methods (see Table S2 and Fig. S4, Fig. S5, and Fig. S6).

Fitness cost of the F plasmid

We observed slight boundary bending in the experimental data, suggesting a fitness cost to the F plasmid. This is consistent with Eq. S7 in the Supporting Material (see also Fig. 5 *C*) and we thus estimated $v_\perp/v_{||} = 0.054$. An analogous procedure was used in simulations (see Table S3).

Quantification of conjugation

In both experiments and simulations, we quantified conjugation by the fraction of the colony circumference occupied by the transconjugant cells (5.2 and 1.6% for 1-μL inoculum grown for four days without and with g3p-N, respectively; see Fig. 3). We emphasize that the number of transconjugant sectors was not used to parameterize
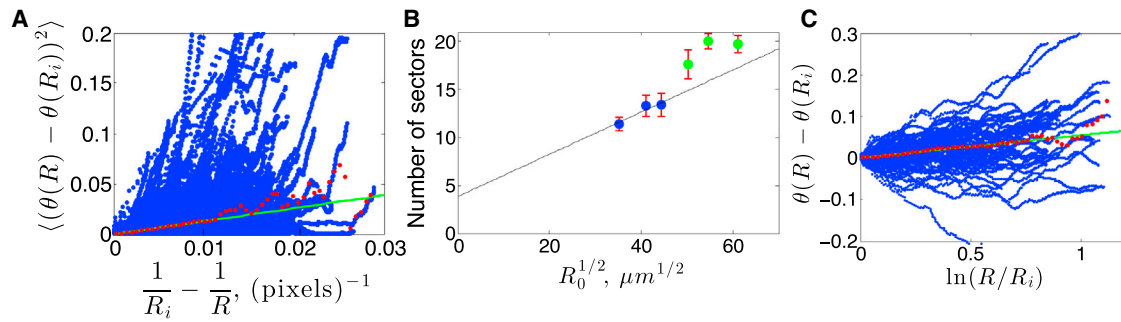
FIGURE 5 Quantification of sector patterns. (*A*) Diffusion of sector boundaries between differently labeled F$^-$ cells of equal fitness was tracked in colonies grown for 18 days. We plotted 1373 individual sector boundaries as a function of radial position R and initial boundary position R_i in blue. The data were then split into 50 bins of equal length and averaged (*red dots*). The least-squares line constrained through the origin, as predicted by Eq. S3 in the Supporting Material, was fit to the first 20 bins, which were not affected by sampling noise. The slope of the fit was used to estimate $D_s/v_{||}$. Pixel size is 50 μm. (*B*) Number of sectors versus $R_0^{1/2}$. Initial radii for the 1, 2, 3, 6, 10, and 15 μL colonies were averaged separately and the mean number of sectors $\pm$ SE was calculated. For the three largest drop sizes (*green*), some very small sectors would likely be annihilated if grown for more time, but further growth would likely have suffered from nutrient deficiency and dehydrating conditions, so the line of best fit was calculated from the 1-, 2-, and 3-μL drop sizes (*blue*) constrained to the slope predicted by Eq. S5 in the Supporting Material with the previously calculated value of $D_s/v_{||}$. The y intercepts from panel *B* and Fig. S7, a second set of colonies, were averaged to 4, providing an estimate of $D_g/v_{||}$. (*C*) The fitness difference between F$^+$ and F$^-$ cells in the absence of tetracycline was measured by plotting the sector boundary deviation as a function of the logarithm of the radial position. Boundaries were defined relative to F$^-$ sectors, and one boundary of each sector was reflected so that all of them twist in the same direction. Most of the 76 sector edges grow outward, corresponding to positive $v_\perp/v_{||}$. The trajectories were split into 50 bins of equal length to obtain the average behavior (*red*). The least-squares line constrained to pass through the origin as predicted by Eq. S7 in the Supporting Material was fit to the first 15 bins (unaffected by sampling noise) to yield $v_\perp/v_{||}$. To see this figure in color, go online.

the model, but instead to check the agreement between experiments and simulations.

Match between experiments and modeling accurately quantifies conjugation

Experimental data were used to parameterize the model as described in the Materials and Methods. The results of this matching are summarized in Table 2 and see also Table S4 and Table S5; visualizations are presented in Fig. S8. Note that we report conjugation rate per unit of time using the relation $r_{exp} = r_{sim} T_{sim}/T_{exp}$ because rT is a dimensionless invariant.

We checked whether the parameterized model was able to correctly predict additional biological results, which had not

been included during parameterization (see Table 2, consistency checks), and obtained the following:

1. We found that the model parameterization successfully captured the inhibition of conjugation by g3p-N protein (Table 2). Using experimental data from the surface-associated populations, the modeling estimated that addition of 10 nM g3p-N reduces the effective conjugation rate by more than a factor of three, from 7.6×10^{-3} h^{-1} to 2.4×10^{-3} h^{-1}. This reduction is similar to previously reported results in liquid culture (5), in which 10 nM g3p-N reduced the rate of transconjugant spread by a factor of 2.5.
2. Another success of the model is the accurate prediction of the number of transconjugant sectors, both with and without g3p-N protein (Table 2, and see Fig. S6 and

TABLE 2 Quantification of conjugation in experiments and simulations

Quantity	Experimental measurement	Simulation quantity	Data utilized
Time	$T = 4$ days	$T_{sim} = 4295$ generations	Time of growth
Length	$L = 1.6$ cm	$L_{sim} = 1015$ demes	Average colony circumference
Migration	$D_s/v_{||} = 32$ μm	$m = 0.05$/generation	Random walk of boundaries
Genetic drift	$D_g/v_{||} = 0.785$	$N = 100$	Number of sectors
Plasmid cost	$v_\perp/v_{||} = 0.054$	$s = 4.5 \times 10^{-4}$	Deterministic bending of boundaries
Conjugation rate without g3p	$r = 7.6 \times 10^{-3}$/h	$r = 1.7 \times 10^{-4}$, unitless	Transconjugant circumference proportion
Conjugation rate with g3p	$r = 2.4 \times 10^{-3}$/h	$r = 5.5 \times 10^{-5}$, unitless	Transconjugant circumference proportion
Consistency check: transconjugant sectors without g3p	2.14 ± 0.31	2.05 ± 0.30	Number of transconjugant sectors
Consistency check: transconjugant sectors with g3p	1.00 ± 0.22	1.00 ± 0.13	Number of transconjugant sectors

All quantities except the conjugation rate were measured in experiments and their simulation counterparts were fit to match the experimental setup. Then, the simulation conjugation rate was fit to the observed transconjugant circumference proportion to determine the experimental conjugation rate. As a consistency check, we observed that the number of sectors in simulations agreed with experimental conditions without and with g3p-N protein even though these values were not used to match the conjugation rate.

Fig. S7), which was not used in parameterizing the model.

Using our model, we explored how the fate of conjugative plasmid depends on the selective coefficient and conjugation rate in spatial populations (Fig. 6 and Fig. S9). As expected, higher conjugation rates facilitated plasmid spread whereas higher fitness costs inhibited it. Our model predicts that the conjugative plasmid is lost when $s > r$ because the fraction of plasmid-free F^- cells depends only on $(s - r)$; see Eq. 7. We expect this result to hold in more complex communities as long as both competition and conjugation occur locally (e.g., along the sector boundaries).

Many natural conjugative plasmids might be living close to an extinction threshold; otherwise, they would either spread rapidly or go extinct. Although the threshold for plasmid spread ($r = s$) is the same in both spatial and well-mixed populations, their evolution is quite different. When $r \approx s$, F^+ cells in well-mixed populations are primarily transconjugants because original F^+ cells are outcompeted. Therefore, genetic background of initially F^+ cells is lost and the conjugative plasmid spreads primarily via horizontal transmission. In contrast, spatial populations would have a much smaller fraction of transconjugants un-

der similar conditions, which is evident from the lack of transconjugant-dominated blue along the $r = s$ diagonal in Fig. 6. In spatial populations, competition and conjugation would occur near the boundaries and the bulk of the original F^+ cells will be shielded from competition with F^- cells. As a result, the genetic background of initially F^+ cells is preserved and vertical transmission is a primary mechanism of plasmid persistence. Such differences are likely to play an important role in the evolution of both bacteria and their conjugative plasmids.

DISCUSSION

We analyzed conjugation of an F plasmid carrying tetracycline resistance in bacterial colonies growing on an agar surface. The genetic history of the colony could be visualized in the fluorescence pattern, which distinguished among donor (F^+_c), potential recipient (F^-), and transconjugant cells. As expected, conjugation events occurred only at boundary zones between F^+ and F^- cells. However, in spatially structured populations, the number of boundary zones was surprisingly small, even when the populations were initially well mixed, because strong genetic drift at the colony edge led to stochastic separation of different strains in space, i.e., genetic demixing. As a result, the F plasmid failed to spread in the population, in sharp contrast to liquid culture, where F^- and F^+ cells easily come in contact and the F plasmid spreads through the population like an epidemic, approaching complete conversion to the F^+ genotype (5).

We have extended previous models of conjugation to include spatial structure and genetic demixing during range expansions in bacterial populations growing on a surface. Stochastic simulations were necessary to capture the important element of genetic drift in the spatially structured environment, because drift determines the availability of zones in which F^+ and F^- cells can contact one another. Our parameterization method using invariants meant that experimental invariants determined simulation invariants with no additional degrees of freedom. Our model makes the simplifying assumptions that conjugation and competition are first-order reactions, and that both donor and transconjugant cells are immediately capable of future conjugation after a conjugation event, although a refractory period is known to follow conjugation events (28,29). We also neglected the circular geometry of the colonies and used discrete demes to model a continuous population. Nevertheless, our simulations based on a one-dimensional stepping-stone model accurately describe experimental outcomes and could be used to estimate the effective conjugation rates from the data.

As noted by others, previous measurements of plasmid transfer rates in surface-associated populations have been difficult to interpret (15). The commonly used endpoint method (30) provides a reliable estimate for
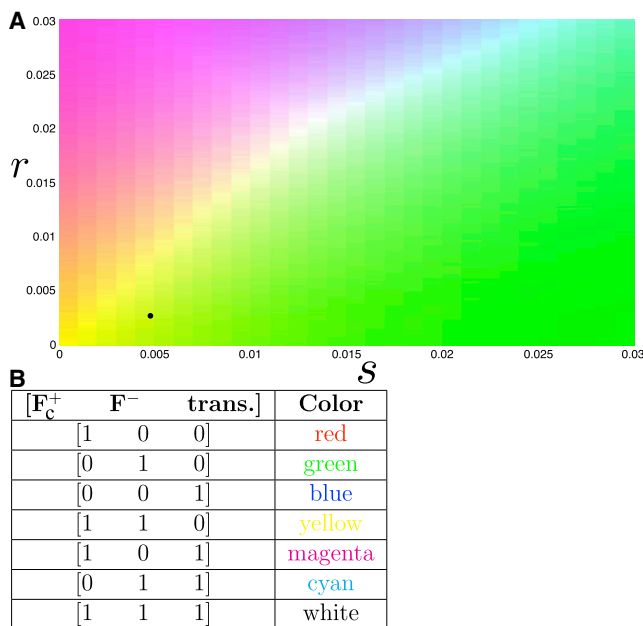

FIGURE 6 Simulation outcome as a function of conjugation (r) and selection (s). (A) Simulations of $N = 30$, $mN = 1$ were conducted over a range of 150 r values from 0 to 0.03 and 30 s values from 0 to 0.03. The values that correspond to four days of experimental growth without g3p are $s = 4.8 \times 10^{-3}$ and $r = 2.63 \times 10^{-3}$ (5.2% transconjugants) as marked (*black dot*). Coloring represents the total fraction of individuals of each type over the entire population at $T_{sim} = 252$ generations: (*green regions*) almost 100% F^- individuals, as expected for high s; (*white regions*) equal mix of F^+_c, F^-, and transconjugants; and (*yellow regions*) 50% F^+ and 50% F^- corresponding to low s and r in which few population-changing events occur. (B) Shading of the relative population composition for each simulation in panel A. To see this figure in color, go online.

B

[F^+_c	F^-	trans.]	Color
[1	0	0]	red
[0	1	0]	green
[0	0	1]	blue
[1	1	0]	yellow
[1	0	1]	magenta
[0	1	1]	cyan
[1	1	1]	white

homogeneously-mixed populations, but it has also been applied to bacterial populations with spatial structure (31–33), for which assumptions of the method are violated. Although any pair of donor and recipient cells can conjugate in a well-mixed population, conjugation is restricted to spatial neighbors in a surface-associated population, where the distribution of donors and recipients on very small spatial scales determines the rate of production of transconjugant cells (31,33,34). The approach taken here incorporates this crucial fact by treating the population as a set of demes connected by nearest-neighbor migration and restricting plasmid transfer only to cells present in the same deme. The important role of stochastic fluctuations, which cause genetic demixing and a qualitative change in conjugation behavior in the population, is also neglected by the endpoint method. Our method includes these effects, and the resulting estimate of the effective conjugation rate could allow quantitative comparisons of transfer efficiencies across different plasmids and environments (13,35,36). Thus, visualization and analysis of expanding and conjugating microbial populations on surfaces is analytically, experimentally, and computationally tractable, enabling in-depth study of the dynamics of gene transfer.

CONCLUSION

Although the F plasmid is the most thoroughly studied conjugative system, many others exist and are medically important in the spread of antibiotic resistance (37). Such systems should be studied in realistic settings, such as surfaces and biofilms, where stochastic effects heavily influence the genetic outcome. Our findings suggest that strategies to enforce spatial structuring could reduce the spread of undesirable genes to new organisms even though the donor cells themselves may continue to reproduce and constitute a large fraction of the microbial population. Such ecological strategies are complementary to attempts to block conjugation at a molecular level. Indeed, we found that spatial structure from surface growth combined with an inhibitor of conjugation produces a multiplicative decrease in the conjugation rate. Such anticonjugation strategies may be worthy of further study as resistance to antibiotics becomes increasingly widespread among pathogenic bacteria.

SUPPORTING MATERIAL

Nine figures, seven tables and supplemental information are available at http://www.biophysj.org/biophysj/supplemental/S0006-3495(14)00080-0.

REFERENCES

1. Davies, J., and D. Davies. 2010. Origins and evolution of antibiotic resistance. *Microbiol. Mol. Biol. Rev.* 74:417–433.

2. Barlow, M. 2009. What antimicrobial resistance has taught us about horizontal gene transfer. *In* Horizontal Gene Transfer: Genomes in Flux. M. Gogarten, J. Gogarten, and L. Olendzenski, editors. Humana Press, Totowa, NJ, pp. 397–411.

3. Waters, V. L. 1999. Conjugative transfer in the dissemination of β-lactam and aminoglycoside resistance. *Front. Biosci.* 4:D433–D456.

4. Boeke, J. D., P. Model, and N. D. Zinder. 1982. Effects of bacteriophage f1 gene III protein on the host cell membrane. *Mol. Gen. Genet.* 186:185–192.

5. Lin, A., J. Jimenez, …, I. A. Chen. 2011. Inhibition of bacterial conjugation by phage M13 and its protein g3p: quantitative analysis and model. *PLoS ONE.* 6:e19991.

6. Król, J. E., H. D. Nguyen, …, E. M. Top. 2011. Increased transfer of a multidrug resistance plasmid in *Escherichia coli* biofilms at the air-liquid interface. *Appl. Environ. Microbiol.* 77:5079–5088.

7. Shoemaker, N. B., H. Vlamakis, …, A. A. Salyers. 2001. Evidence for extensive resistance gene transfer among *Bacteroides* spp. and among Bacteroides and other genera in the human colon. *Appl. Environ. Microbiol.* 67:561–568.

8. Hausner, M., and S. Wuertz. 1999. High rates of conjugation in bacterial biofilms as determined by quantitative in situ analysis. *Appl. Environ. Microbiol.* 65:3710–3713.

9. Fox, R. E., X. Zhong, …, E. M. Top. 2008. Spatial structure and nutrients promote invasion of IncP-1 plasmids in bacterial populations. *ISME J.* 2:1024–1039.

10. Christensen, B. B., C. Sternberg, and S. Molin. 1996. Bacterial plasmid conjugation on semi-solid surfaces monitored with the green fluorescent protein (GFP) from *Aequorea victoria* as a marker. *Gene.* 173 (1 Spec No):59–65.

11. Reisner, A., H. Wolinski, and E. L. Zechner. 2012. In situ monitoring of IncF plasmid transfer on semi-solid agar surfaces reveals a limited invasion of plasmids in recipient colonies. *Plasmid.* 67:155–161.

12. Ellis, R. J., A. K. Lilley, …, H. C. Godfray. 2007. Frequency-dependent advantages of plasmid carriage by *Pseudomonas* in homogeneous and spatially structured environments. *ISME J.* 1:92–95.

13. Sørensen, S. J., M. Bailey, …, S. Wuertz. 2005. Studying plasmid horizontal transfer in situ: a critical review. *Nat. Rev. Microbiol.* 3:700–710.

14. Nowak, M. A. 2006. Evolutionary Dynamics: Exploring the Equations of Life. Harvard University Press, Cambridge, MA.

15. Zhong, X., J. Droesch, …, S. M. Krone. 2012. On the meaning and estimation of plasmid transfer rates for surface-associated and well-mixed bacterial populations. *J. Theor. Biol.* 294:144–152.

16. Liu, C., J. Krishnan, and X. Y. Xu. 2013. Investigating the effects of ABC transporter-based acquired drug resistance mechanisms at the cellular and tissue scale. *Integr. Biol. (Camb.)* 5:555–568.

17. Lagido, C., I. J. Wilson, …, J. I. Prosser. 2003. A model for bacterial conjugal gene transfer on solid surfaces. *FEMS Microbiol. Ecol.* 44:67–78.

18. Simonsen, L. 1990. Dynamics of plasmid transfer on surfaces. *J. Gen. Microbiol.* 136:1001–1007.

19. Krone, S. M., R. Lu, …, E. M. Top. 2007. Modeling the spatial dynamics of plasmid transfer and persistence. *Microbiology.* 153:2803–2816.

20. Hallatschek, O., P. Hersen, …, D. R. Nelson. 2007. Genetic drift at expanding frontiers promotes gene segregation. *Proc. Natl. Acad. Sci. USA.* 104:19926–19930.

21. Birge, E. A. 2006. Bacterial and Bacteriophage Genetics. Springer, New York.

22. Kimura, M., and G. H. Weiss. 1964. The stepping stone model of population structure and the decrease of genetic correlation with distance. *Genetics.* 49:561–576.

23. Korolev, K. S., M. Avlund, …, D. R. Nelson. 2010. Genetic demixing and evolution in linear stepping stone models. *Rev. Mod. Phys.* 82:1691–1718.

24. Korolev, K. S., J. B. Xavier, …, K. R. Foster. 2011. A quantitative test of population genetics using spatiogenetic patterns in bacterial colonies. *Am. Nat.* 178:538–552.

25. Moran, P. A. P. 1962. Statistical Processes of Evolutionary Theory. Clarendon Press, Oxford, UK.

26. Korolev, K. S., M. J. I. Müller, …, D. R. Nelson. 2012. Selective sweeps in growing microbial colonies. *Phys. Biol.* 9:026008.

27. Zünd, P., and G. Lebek. 1980. Generation time-prolonging R plasmids: correlation between increases in the generation time of *Escherichia coli* caused by R plasmids and their molecular size. *Plasmid.* 3:65–69.

28. Cullum, J., J. F. Collins, and P. Broda. 1978. Factors affecting the kinetics of progeny formation with F'lac in *Escherichia coli* K12. *Plasmid.* 1:536–544.

29. Andrup, L., L. Smidt, …, L. Boe. 1998. Kinetics of conjugative transfer: a study of the plasmid pXO16 from *Bacillus thuringiensis* subsp. *israelensis*. *Plasmid.* 40:30–43.

30. Simonsen, L., D. M. Gordon, …, B. R. Levin. 1990. Estimating the rate of plasmid transfer: an end-point method. *J. Gen. Microbiol.* 136:2319–2325.

31. Normander, B., B. B. Christensen, …, N. Kroer. 1998. Effect of bacterial distribution and activity on conjugal gene transfer on the phylloplane of the bush bean (*Phaseolus vulgaris*). *Appl. Environ. Microbiol.* 64:1902–1909.

32. Lilley, A. K., and M. J. Bailey. 2002. The transfer dynamics of *Pseudomonas* sp. plasmid pQBR11 in biofilms. *FEMS Microbiol. Ecol.* 42:243–250.

33. Licht, T. R., B. B. Christensen, …, S. Molin. 1999. Plasmid transfer in the animal intestine and other dynamic bacterial populations: the role of community structure and environment. *Microbiology.* 145:2615–2622.

34. Haagensen, J. A., S. K. Hansen, …, S. Molin. 2002. In situ detection of horizontal transfer of mobile genetic elements. *FEMS Microbiol. Ecol.* 42:261–268.

35. Shu, A. C., C. C. Wu, …, T. R. Yew. 2008. Evidence of DNA transfer through F-pilus channels during *Escherichia coli* conjugation. *Langmuir.* 24:6796–6802.

36. Babic, A., A. B. Lindner, …, M. Radman. 2008. Direct visualization of horizontal gene transfer. *Science.* 319:1533–1536.

37. Costelloe, C., C. Metcalfe, …, A. D. Hay. 2010. Effect of antibiotic prescribing in primary care on antimicrobial resistance in individual patients: systematic review and meta-analysis. *BMJ.* 340:c2096.